

Biochar based cathode enriched with hydroxyapatite and Cu nanoparticles boosting electromethanogenesis

G. Ghiara^a, S. Campisi^b, A. Goglio^c, F. Formicola^d, M. Balordi^e, A. Gervasini^b, S.P.M. Trasatti^a, F. Adani^c, A. Franzetti^d, P. Cristiani^{e,*}

^aDepartment of Environmental Sciences and Policy (ESP), Università degli Studi di Milano, Via C. Golgi 19, 20133, Milano, Italy

^b Department of Chemistry, Università degli Studi di Milano, Via C. Golgi 19, 20133, Milano, Italy

^c Department of Agriculture and Environmental Sciences (DiSAA), Università degli Studi di Milano, Via Celoria 2, Milano, Italy

^d Department of Earth and Environmental Sciences (DISaT), University of Milan Bicocca, Piazza della Scienza 1, 20126, Milano, Italy

^eRSE-Ricerca sul Sistema Energetico S.p.A., Via Rubattino 54, 20134 Milano, Italy

*corresponding author: pierangela.cristiani@rse-web.it

Abstract

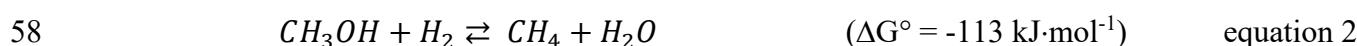
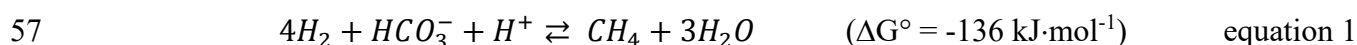
Electromethanogenesis is an innovative technology addressing the need of storing renewable energy from unprogrammable sources. It allows for the electrochemical production of methane from CO₂-rich wastes on microbial cathodes, in a logic of power-to-gas (BEP2G). The challenge of cost-effective and sustainable biocathodes enhancing the microorganism performance and yield of electromethanogenesis is approached in this work. For the first time, porous carbonaceous cathodes were functionalized with Cu nanoparticles and hydroxyapatite (HAP) and successfully experimented for supporting microbial CO₂ reduction reaction (CO₂RR) to methane. Tests were performed in a double chamber system under CO₂ flow at 45 °C. Next Generation Sequencing of 16S RNA indicated that the microbial pool on the cathodes was mostly enriched in Metanobacteriaceae (hydrogenotrophic Archaea) and different fermenting bacteria, depending on the cathode type. High methane production on cathodes made of Cu 20%, HAP 10%, and carbon balance (20Cu/10HAP) was achieved, with a maximum of 866±199 mmol m⁻² d⁻¹ (projected cathode area, Coulombic efficiency of 64%), corresponding to values comparable to the maximum in literature, but in shorter timespans (8 vs 30 days). The documented effect of pH stabilization in the cathodic chamber by HAP was one of the main parameters that concurred to the selectivity of CO₂RR towards methane.

Keywords: Electromethanogenesis, HAP, CO₂RR, Bioelectrolyses, BES, Hydrogenotrophic Archaea.

1. INTRODUCTION

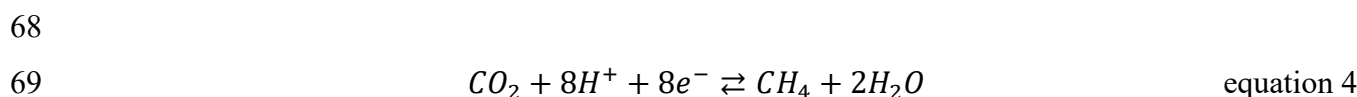
36 Electromethanogenesis [1, 2], consisting of the reduction of CO₂ in the form of methane (CH₄) *via*
 37 microbial electrolysis [3-4], is a valuable alternative to both biochemical methanogenesis and
 38 thermochemical methanation from the Sabatier process [5-6]. Among the innovative technologies for
 39 energy conversion, the peculiarity of this bioelectrochemical process is to address the need of storing
 40 the energy produced from unprogrammable sources in renewable fuel (hydrogen or methane), in a
 41 power-to-gas concept (BEP2G) [1, 5-9]. Although such processes address marginal energy resources,
 42 their study finds valuable meaning in promoting a green circular economy by producing new
 43 biomethane or upgrading biomethane and CO₂ from anaerobic digestion (AD) in the already operating
 44 biogas plants [7]. In Italy, about 1600 biogas plants were operative in 2019, making this country the
 45 2nd country for biogas production in the EU and the 4th worldwide [10]. The potential of biomethane
 46 production has been estimated at 10 billion cubic meters by 2030, which means that about 8 billion
 47 cubic meters of CO₂ will be produced by 2030, i.e. about 15·10⁶ tons of CO₂, assuming a biogas
 48 composition, as average, of 45 % CO₂ (v/v) and 55 % CH₄ [11]. CO₂ produced by biogas/biomethane
 49 plants does not contribute to greenhouse gases (GHG) because it comes from renewable biomass and
 50 therefore, its recovery as feedstock can reduce GHG emission balancing fossil-origin emitted CO₂ (C
 51 trading). For Italy, it is possible to calculate a theoretical recovery of 15·10⁶ tons of CO₂ from biogas
 52 by 2030, i.e. 4 % of the total emitted CO₂ (348.4 Mtons, [10, 11]).

53 The mechanisms of CH₄ biochemical production follow specific metabolic pathways ascribed to
 54 selected species of microorganisms [12-16]. From a thermodynamic point of view, the reaction of
 55 CH₄ production is driven by the type of substrate and the energy source according to their values of
 56 Gibbs free energy at standard conditions (25 ° C and pH 7), as displayed by the following reactions:



60 In brief, it is possible to discern two main pathways for methanogenesis: i) hydrogenotrophic one,
 61 which involves the reduction of carbonate ions (equation 1), the most metabolically efficient process
 62 for energy generation [17, 18]; ii) acetoclastic pathway, which consumes acetate ions or methanol,
 63 (equations 2 and 3).

64 Both these pathways (more relevantly the acetoclastic one) occur during the anaerobic digestion (AD)
 65 in the biogas process producing methane. In the BEP2G process, the sole hydrogenotrophic
 66 microorganisms of the Archaea domain - the same as in the biogas plants - produce methane on a
 67 polarized electrode around -1V vs the Standard Hydrogen Electrode (*SHE*) [12] (equation 4):



70
71 CH₄ forms, catalysed by microorganisms, directly on the biocathode or indirectly after the hydrogen
72 evolution reaction [1]. Methanogenesis can be catalysed using only CO₂ and bicarbonate that can be
73 coupled to both the oxidation of water and the abiotic, or microbial, oxidation of organic molecules
74 [19-20]. In both cases, the end products of metabolic pathways are methane and water.

75 Combining microbial electromethanogenesis with conventional AD, the upgrading of biomethane
76 produced in biogas plants (rich in CO₂ up to 45%) can be achieved [7]. Several other CO₂-rich
77 industrial wastes would reach a technological upgrade towards a more circular economy by
78 electromethanogenesis. However, important challenges concerning methane yield from this
79 technology, still approached at the laboratory level only, are persisting [20-23]. Previous studies are
80 mainly focused on the optimization of the chamber set-up (i.e., single, or double chamber) [2], applied
81 cathode potential, choice of microorganisms, cathode and/or anode feeding, pH, and other process
82 parameters [24-26]. To scale up BEP2G energy storage system to a possible economically and
83 industrially competitive level, the study of performing materials for the cathode is generally agreed
84 upon as mandatory. Electrodes must give large surfaces to maximize the interaction with
85 microorganisms, minimizing charge transfer resistance and diffusive mass transport [26]. One of the
86 main challenges for increasing the performance of electromethanogenesis, compared to the chemical
87 electrolysis of water, consists of manufacturing electrodes with a geometric surface equal to at least
88 one order of magnitude greater than the volume of the bioreactor (ratio of 10 m²·m⁻³) [27]. This
89 indication is useful to counterbalance the low current density sustained by microorganisms. Metallic
90 materials that can chemically support microorganisms for reaching a suitable performance of the
91 electrodes in bioelectrochemical systems (BES) are very expensive (e.g. Pt group) or tend to suffer
92 from microbial corrosion. Sometimes this last phenomenon can greatly invalidate the data of methane
93 electrochemical production, as reported by literature [28]. The choice of a more cost-effective
94 material drove recent research toward carbon of biological origin (biochar) [28-30], which assures
95 high porosity, good conductivity, high biocompatibility, acceptable mechanical strength, and
96 resilience. Biochar is generally characterized by a high specific surface (reaching 100 m²·m⁻³) with a
97 porosity and pore size distribution that makes its surface entirely available for extracellular electron
98 transfer by microbes [31, 32]. The performance of biochar can, therefore, in principle, approach that
99 of an ideal electrode to produce CH₄, as confirmed by recent studies [33, 34].

100 To further enhance the chemical reduction reaction of CO₂ (CO₂RR), enriched layers of metallic
101 catalysts can be applied on the surface of the cathode [35-37]. Among the active phases, Cu presented
102 encouraging results (around 40%) towards CO₂RR at applied potentials of -1.2 V vs RHE [38] and
103 Cu-based nanostructures have also been shown to generate CH₄, with different faradaic efficiencies

104 depending on the shape, size, and supports of copper nanoparticles (CuNPs) [39, 40]. However,
105 studies indicate a low selectivity of Cu towards the CH₄ formation. Therefore, materials alternative
106 to metals are currently explored [41, 42]. Relevantly, it was recently demonstrated that phosphates
107 in the nanocrystalline form of hydroxyapatites (HAP) can show good absorption toward CO₂ [43,
108 44]. HAPs are green materials widely distributed in nature and the principal component of the bones
109 [43,44]. In a nanocrystalline structure, they are characterized by acidic and basic sites that can
110 catalytically trigger the CH₄ production [45, 46]. Particularly, the combined presence of CuNPs and
111 HAP has a synergistic effect on the CO₂RR to CH₄ as CuNPs allows the direct reduction of CO₂
112 (transfers > 2 e-) to a wide range of so-called higher-order products (as CH₄, C-2 or C-3) [47].
113 In this work, for the first time to our knowledge, an innovative biochar-based material functionalized
114 with CuNPs and HAP is studied and tested for enhancing the biocathode performance in
115 electromethanogenesis. The addition of hydroxyapatite is supposed to introduce additional basic sites
116 complementary to those exhibited by the biochar [43]. Furthermore, the presence of acidic sites is
117 supposed to stabilize pH. Low-cost solid electrodes of biochar (biogenic carbon) were produced from
118 the pyrolysis of maize stalk and then enriched with different wt. percentages of Cu nanoparticles and
119 HAP (5Cu/5HAP and 10Cu/20HAP). Samples with only Cu and HAP were also produced and tested
120 as control. The preparation of the electrode materials requested an innovative multi-step protocol here
121 described in detail. The performance of CuNPs/HAP functionalized biochar is also compared with
122 carbon cloth, as the best performance in terms of methane production from literature has been
123 reported with this carbon material [19].

124

125 **MATERIALS AND METHODS**

126 Six different carbon-based cathodes, described and named as in Table 1, were experimented with
127 double-chamber electrochemical cells.

128 Commercial CuNPs (SigmaAldrich, CAS 7440508, $\sigma = 25$ nm) and HAP produced at the University
129 of Milan, according to a procedure described elsewhere [48], were used as additives of carbon
130 powders achieved by pyrolysis of plant residues.

131 For carbon cloth, a commercial product (*SAATI*, Legnano, Italy) was used. The other carbonaceous
132 materials were prepared in the lab, following a protocol consisting of three steps (Fig. S1,
133 Supplementary material).

134 *First step: preparation of the biochar.* Biochar was produced from the pyrolysis of maize stalk. To
135 obtain an electrically conductive material, the canes were positioned in a quartz tube inside a
136 horizontal furnace (Carbolite) and pyrolyzed at controlled temperature. The pyrolysis procedure of
137 the material was carried out according to the following protocol: two h at 25 °C, slow heating (5

138 °C·min⁻¹) up to 900 °C, one h residence time at 900 °C and cooling down to 25 °C. During the
139 treatment, N₂ flowed constantly at 1 NL·h⁻¹. This type of procedure allows fast heating and maximum
140 treatment efficiency, without any heat loss [30].

141 Second step: preparation of the functionalized powder. Four biochar based powders of different
142 compositions were synthesized and labelled according to the weight percentage of each component
143 of the carbon powder as described in Table 1.

144 Firstly, biochar was pulverized using an agate mortar. Then, the powder was mixed in a solution
145 containing different concentrations of copper nanoparticles. To obtain the 20Cu powder
146 approximately 85 of biochar was dispersed in ca. 40 ml of isopropyl alcohol (IPA). The pH of the
147 suspension was adjusted to 10 by adding an aqueous solution of 0.1 M KOH. Approx. 25 of
148 commercial CuNPs were dispersed in ca. 40 mL of IPA, adjusting the pH as indicated for the biochar
149 suspension. Both mixtures were placed in ultrasounds for 30 minutes to obtain optimal suspensions.
150 Then, the CuNPs suspensions was added one shot to the biochar suspension. The resulting mixture
151 was stirred at room temperature for 48 h (Fig. S1, Supplementary material). After the immobilization
152 step, the powder was vacuum filtered on a 0.45 m Nylon membrane, washed with MilliQ water and
153 dried at 110 ° C for 45 minutes.

154 The same procedure was used to obtain the powder 5Cu, weighing around 95 mg of biochar and 7
155 mg of CuNPs, respectively.

156 To obtain the powder 10HAP, nanocrystalline hydroxyapatite was added by co-precipitation to the
157 biochar powder. Approximately 90 mg of biochar were suspended in ca. 90 ml of MilliQ water. The
158 pH of the suspension was brought to 7 by adding a 0.1 M aqueous solution of KOH. Similarly, ca. 15
159 mg of HAP were dispersed in ca. 20 mL of MilliQ water, adjusting the pH of the suspension to 7 by
160 adding a 0.1 M KOH solution. Both mixtures were sonicated for 45 minutes. Then, the HAP
161 suspension was added one shot to the biochar suspension. the resulting mixture was stirred for 48 h
162 at room temperature. Finally, the powder was vacuum filtered on a 0.45m Nylon membrane, washed
163 with MilliQ water, and dried at 110 ° C for three hours (Fig. S1, Supplementary material).

164 To obtain the composite 20Cu/10HAP the already mentioned procedure for HAP was applied,
165 replacing the undoped biochar with the already synthesized composite 20Cu. Analogously, to produce
166 the composite 5Cu/5/HAP, 5Cu was used, weighing around 100 mg of 5Cu powder and 7 mg of HAP.

167 Third step: application of the powder to the electrode. The final step involved enriching the biochar
168 support with powder functionalized with the four composites obtained. The resulting tested composite
169 material were labelled according to the percentages of the synthesized powder (Table 1). Similar to
170 the composite powder alone, the percentage value of copper and hydroxyapatite both express the
171 gravimetric ratios vs. biochar. For the application of the powder on the carbonaceous material, a dip

172 coating procedure was carried out. It consisted in immersing the previously pyrolyzed biochar in an
173 aqueous solution (100 mL for 100 mg of powder) of the four composites (10HAP, 20Cu, 5Cu/5HAP
174 20Cu/10HAP obtained by co-precipitation as previously described. Solutions were first sonicated for
175 ten minutes to achieve good mixing and the biochar was immersed in the solution for ten
176 minutes (Fig. S1, Supplementary material). The electrode thus obtained was dried at 110 ° C for three
177 h.

178 **2.2 Experimental setup**

179 Two apparatus of six double-chamber BESs were operated in parallel. A schematic of the
180 electrochemical cell is reported in Figure 1a. Images of operating cells are shown in Figure 1b and
181 1c. Each apparatus was equipped with: i) a thermostatic tank containing BESs; ii) a controlled CO₂
182 flow system; iii) a current generator, equipped with six independent channels each one connected to
183 the anode and cathode of each BES, designed by AMEL s.r.l. (Milano, Italy).

184 A reference electrode 3M Ag/AgCl was inserted in each cathodic compartment. A polarization
185 between the anode and cathode was imposed in order to achieve -1.2 V between the cathode and
186 reference (approximately -1 V vs SHE) of each BES.

187 The current circulating between the anode and the cathode was estimated by measuring voltage across
188 an electrical resistance of 10 Ω connected in series with the anode (Fig. 1a) [49]. The recording of
189 voltages was performed with an analog to digital acquisition board (Agilent 4930 A data-logger). The
190 duration of the experiments was 200 h (8 days) and was replicated twice. For each material, also an
191 abiotic condition was tested.

192 The double-chamber BESs were made of borosilicate (Pyrex) bottles and were operated at 45 ± 1° C.
193 The anodic and cathodic chambers were separated by a proton exchange membrane (PEM NAFION
194 417) with a working surface of 7.0 cm². Each chamber was filled with about 0.200 L of solution and
195 was hermetically sealed with a rubber stopper, that hosted the gas dosing and vent pipes, the reference
196 electrodes, the electrode current collectors, and the steel needles for gas sampling (Fig. 1a).

197 The anode was a Ti-mesh of a suitable area of 36 cm² connected to a Ti current collector (ø = 1 mm).
198 The cathodes, made with one of the six different materials under investigation (Table 1), were fixed
199 with an electrolytic copper wire (99.9%) acting as a current collector.

200 The anolyte was a 0.2 M solution of Na₂SO₄. The catholyte solution consisted of the inoculum
201 retrieved from a biogas plant and stored at the University of Milan, Bicocca. The inoculum was
202 supplied with 2.54 g · L⁻¹ KH₂PO₄, 11.7 g · L⁻¹ Na₂HPO₄ · 12H₂O, 0.53 g · L⁻¹ NH₄Cl, 0.1 g · L⁻¹ Na₂SO₄,
203 5.0 g · L⁻¹ NaHCO₃, and vitamins.

204 CO₂ was fluxed at each cathode through sparging at the beginning of the experiment for 40 minutes
205 at a flux of 0.5 NL·h⁻¹ (total of 14.8 mmol dosed). The apparatus also automated the CO₂ dosage and
206 the sampling of the gases produced.

207

208 **2.3 Material characterization techniques**

209 To verify the morphology and the pore size of the pyrolyzed biochar and to characterize the biochar
210 powder (and the final functionalized biochar electrode) different analytical methods were performed.

211 A Scanning Electron Microscopy analysis (SEM) coupled with Energy dispersive X-Ray
212 measurements (EDS) was carried out at the Department of Earth Sciences of the University of Milan
213 using a SEM-EDS JSM-IT500 LV (JEOL S.p.a.). The analyses were conducted using a secondary
214 electrons (SE) detector at different magnifications and with an accelerating voltage of 20 KeV and a
215 WD of 10.5 mm. Image analysis was executed using the Software Fiji-ImageJ, version 1.49b [50] to
216 estimate the volume percentage of the composite on the surface of the biochar.

217 X-Ray powder diffraction (XRPD) patterns have been collected using a Philips PW3020/PW1830
218 powder diffractometer operating with an X-ray source at 40 kV and 40 mA in the range between 5 °-
219 60 °(2θ), step of 0.02 °2θ and scan rate of 0.6°·min⁻¹.

220 Electrochemical analyses were performed to determine the electrochemically active surface area
221 (ECSA) of each material. To this purpose, electrically conductive disks of 1 cm² were prepared and
222 immersed in an aerated solution of 0.1M KNO₃. A typical three electrode cell was employed with the
223 cathode as the Working Electrode (WE) a 3M Ag/AgCl as a Reference Electrode (RE) and a platinum
224 wire as a Counter Electrode (CE). Cyclic voltammograms (CV) were recorded at different scan rates
225 (from 10 to 200 mV/s) with an Ivium Compactstat (Ivium Technologies, Netherlands). The scanned
226 range was ± 25mV vs OCP and the double layer capacitance, C_{dl}, proportional to the ECSA, was
227 determined. All CVs were conducted in duplicate.

228

229 **2.4 Chemical analyses**

230 The composition of the produced biogas (CH₄, H₂, and CO₂) was analysed using a gas chromatograph
231 (Agilent 3000A micro-GC) with the software “SOPRANE”. The sample for the GC was taken from
232 the headspace of the cathode chamber with gas bags of 5 L connected to the gas outlet. Gas samplings
233 were carried out at the end of the test. The amount of CH₄ produced was analysed as a concentration
234 of gas sampled in a 5L gas bag and the methane value was normalized to the cathode projected area.
235 Furthermore, the pH was monitored on a three-day basis using three narrow range pH indicator
236 papers.

237 The Volatile Fatty Acids (VFAs) present in the initial inoculum solution and produced at end of the
238 test were analysed by Ionic Chromatography (IC, Dionex 300), equipped with a S9-SC column and
239 chemical suppressor AMMSIC. The sample intended for the analysis through IC (10 mL) was
240 withdrawn using a sterile syringe and stored at 2°C before the measurement.

241 At the end of the test microbial communities grown on the surface of the electrodes were
242 characterized through visual inspection and microscopy observation by scanning electron microscopy
243 equipped with X-Ray detector (SEM-EDS).

244

245 **2.5 Microbiological sampling and analysis**

246 Small size pieces of the cathodes and 3 mL of cathodic media were sampled from each
247 bioelectrochemical system before and after the test. Samples were stored at -26°C before analyses.

248 The sequencing of V5-V6 16S RNA genes of Bacteria and Achaea were carried out on the initial
249 inoculum and on the sampled operated cathodes using MiSeq Illumina sequencing, to obtain the
250 taxonomic characterization of the microbial communities. Total bacterial DNA was extracted using
251 the FastDNA Spin for Soil kit (MP Biomedicals, Solon, OH, USA) and the V5-V6 hypervariable
252 regions of the 16S rRNA gene was amplified through a PCR with initial denaturation at 94°C for 5
253 min, 30 cycles at 94°C for 50 s, 47°C for 30 s, and 72°C for 30 s and a final extension at 72°C for 5
254 min. The reaction was performed in 2.50 µL volume reactions with GoTaq® Green Master Mix
255 (Promega Corporation, Madison, WI, USA) and 1 µM of each primer (783F: 5'-
256 CAGGATTAGATACCC-3', 1027R: 5'-CGACRRCCATGCANACCT-3'). Both primers included
257 barcodes and sequencing adapter fused to the 5' end. The resulting amplicons were purified from 1%
258 agarose gel using Wizard SV Gel and PCR Clean-up System kit (Promega Corporation, Madison, WI,
259 USA). Resulting DNA was quantified using Qubit® (Life Technologies, Carlsbad, CA, USA). The
260 obtained sequences were taxonomically classified by RDP classifier (confidence >80%).

261

262 **3 RESULTS**

263 **3.1 Cathodes characterization**

264 *Pyrolyzed biochar*

265 Firstly, maize stalk samples were weighted before and after pyrolysis to verify the success of the
266 procedure. Fig. 2 shows representative pictures of a sample before and after the treatment.

267 The material after pyrolysis maintained the same mechanical structure and highlighted an increasing
268 number of pores on the surface. A weight loss corresponding to approximately 75% of the initial
269 weight was measured for all samples, consistent with the decomposition of the material in the absence
270 of oxygen. During this process, the lignocellulosic components such as cellulose (C₆H₁₀O₅) n-

271 hemicellulose and lignin undergo depolymerization reactions, fragmentation, and cross-linking [51].
272 This treatment was carried out to increase the porosity of the material and the surface area by several
273 orders of magnitude [51]. Porosity is formed because of the loss of water during the treatment.
274 Generally, three types of pores can be distinguished according to the final application of the biochar:
275 i) micropores (<2nm); ii) mesopores (2-50 nm); ii) macropores (> 50 nm). As displayed in Fig. 2, the
276 material is mainly composed of macropores, with average dimensions around $50 \pm 10 \mu\text{m}$. After the
277 pyrolysis treatment, the presence of macropores can enhance i) the diffusion of gases (CO_2 and H_2)
278 inside the material, also allowing for a good wettability by the H_2O ; ii) the settlement of microbes
279 that catalyses the direct reduction reaction of CO_2 into CH_4 by extracellular electron transfer.

280 Functionalized biochar powder

281 Functionalized biochar powder samples (20Cu, 10HAP, 5Cu/5HAP and 20/10HAP) were
282 qualitatively characterized by SEM-EDS. Fig. 3 shows two images of the two Cu/HAP powders at
283 2000x with relative EDS spectra.

284 From a first observation, it is possible to highlight the presence of micrometric crystals that are
285 distributed on the surface of the biochar (large flakes). They arrange as agglomerates of different type
286 and size and tend to grow around a nucleation centre. These structures bear the typical morphology
287 of HAP adsorbed on the surface of a substrate [52]. Compositional spectra were carried out in some
288 of these areas: spectra 1 and 2 of Fig. 3 indicate a high percentage of C, attributed to the biochar, and
289 the signals of Cu, Ca, O, and P, confirming the presence of elements characteristics of HAP. It was
290 not possible to quantify the overall percentage of the single components due to limits connected to
291 the massive presence of C as substrate (as indicated by the different intensities of the elements in the
292 analysed points). The elemental mapping (Fig. S2, Supplementary information) also shows a good
293 and homogeneous distribution of the elements in the sample with the higher percentages of Cu and
294 HAP (20/10). The composite with a lower presence of the active phase and the dopant (5Cu/5HAP)
295 did not show a total overlap of the signals for the elements Cu, Ca, P and O.

296 Further investigations via XRD were carried out to qualitatively assess the phase composition of
297 materials. The XRPD patterns of 5Cu/5HAP and 20Cu/10HAP (Fig. S3 of Supplementary material)
298 were dominated by a broad peak at 2θ of 20° – 30° which can be ascribed to the (002) plane of aromatic
299 layers that indicate the presence of small graphitic domains in the biochar structure [53]. In addition,
300 typical reflections of bulk Cu (JCPDS 01-070-3038) at 2θ of 43.2° (111) and 50.0° (200) confirmed
301 the presence of copper nanoparticle in the metal form, whereas the peak at 36.5° may be associated
302 to the (111) plane of cubic Cu_2O (JCPDS 00-065–3288), thus suggesting a partial oxidation of Cu.
303 On the other hand, the successful incorporation of hydroxyapatite in the composites was confirmed
304 by the emergence of the most intense reflections of crystalline hydroxyapatite (26° and 32° in

305 agreement JCPDS 00-064-0738). The relative intensities of the graphite, Cu and HAP peaks for each
306 XRD pattern also confirm a different percentage of the agents in the composite.

307 Composite electrode

308 Once the dip coating procedure was terminated, the final electrode was characterized through SEM-
309 EDS. Fig. S4, Supplementary information displays pictures of the Cu/HAP functionalized cathodes
310 (b, c, e and f) compared to the undoped biochar (a, d).

311 Analyses show a good dispersion of the functionalized biochar powders on the electrode surface and
312 particularly both on the pores and on the cell walls. Consistent with the previous observations, a
313 substrate of organic material (biochar), is found below the aggregates of Cu/HAP crystals, visible as
314 white spots (red arrows) in Fig. S4, Supplementary information. The elemental maps (Fig. 4) show a
315 good dispersion of the Cu/HAP composite on the electrode surface even if in much lower percentages
316 than that obtained on the powder. By calculating the total volume percentage of functionalized
317 powder *via* image analysis, it was possible to infer that it constituted less than the 10 % of the total
318 surface for both the composite electrodes.

319 **3.2 Electrochemical behaviour of the electrodes**

320 The electrochemically active surface (ECSA) of the composite electrodes was determined in the range
321 ± 25 mV vs OCP hypothesizing that no faradaic reaction (exchange of electrons) occurs (see Figure
322 S5, supplementary information for the CV curves). This technique is based on the double layer delays
323 in charging and discharging at the interface electrode/solution according to the potential scan-rate
324 [54]. The measured parameter is defined as double layer capacitance (C_{dl}):

$$325 \quad C_{dl} = \varepsilon A/d \quad \text{equation 5}$$

326 where ε is the absolute permittivity of the dielectric material used, A is the area of the electrode and
327 d is the distance between the plates in a pure capacitor (here the interface electrode/electrolyte) [55].
328 Assuming ε and d as constants, the C_{dl} is only affected by the area of the electrode (the larger the
329 electrode, the higher the double layer capacitance). This parameter (C_{dl}) can be thus calculated
330 applying different potential scan-rates (ν) and measuring the resulting current output, defined as
331 double layer charging current (i_c) (equation 6):

$$332 \quad i_c = \nu \cdot C_{dl} \quad \text{equation 6}$$

333 By the slope of the scan rate (ν_s) vs the capacitive current (i_c) graph, the C_{dl} was obtained and ECSA
334 was calculated from the following equation:

$$335 \quad ECSA = C_{dl}/C_s \quad \text{equation 7}$$

336 where C_s is the specific capacitance of the material. To our knowledge, the C_s of this specific biochar
337 is still unknown, so a plausible value of $7.5 \mu\text{F cm}^{-2}$ was selected, based on studies on other carbon-
338 based materials [56-59]. The same value of C_s was considered for all cases (Biochar, 20Cu, 10HAP,

339 5Cu/5HAP, 20Cu/10HAP) giving the low quantities of dopants in the final electrode (<10% volume
340 percentage from the SEM). The results from the ECSA analyses indicated different electrochemically
341 active surfaces according to the type of electrode considered, as visible from Table 2.

342 The pure biochar exhibits the highest ECSA and values up to two orders of magnitude lower are
343 measured for the other composites. It appears that the active phase Cu, if present in high percentages
344 in the synthesized powder (20 wt. %), greatly decreases the electrochemically active surface (10^{-2} cm²
345 for biochar compared to 10^{-4} cm² for 20Cu). On the other hand, the presence of the sole dopant
346 HAP mildly lowers the active surface of the electrode (one order of magnitude). In the composites
347 with both Cu and HAP, the role of hydroxyapatite on the electrochemically active surface is less
348 obvious and a synergistic effect of both Cu and HAP must be considered.

349

350 **3.3 Bioelectrochemical tests**

351 Methane production

352 The production of methane was affected by the nature and functionalization of the cathode. Fig. 5
353 reports the results of the GC analyses after 200 h, displaying the moles of CH₄, H₂ and CO₂ found in
354 the gasbags, normalized per L and for the projected surface area of the cathode. CC and undoped
355 biochar show a very different production of CH₄, observing a consistent increase for the latter (3 and
356 $13 \mu\text{mol} \cdot \text{cm}^{-2} \cdot \text{L}^{-1}$, respectively). Cu in the biochar (composite 20Cu) lowers the average production
357 of CH₄, which results comparable to the CC. The presence of HAP leads to a 3-fold-increase
358 compared to pure biochar (and 10 times vs CC). The combined effect of Cu and the HAP was
359 evidenced in the cathodes functionalized with the highest percentages(20Cu/10HAP), whose methane
360 production reached $70 \mu\text{mol} \cdot \text{cm}^{-2} \cdot \text{L}^{-1}$. On the other hand, the 5Cu/5HAP functionalization was
361 ineffective.

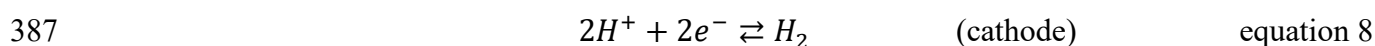
362 The CO₂ and H₂ moles were also measured to understand the chemical pathways of CO₂RR. Medium
363 to high levels of CO₂ was found in all systems (ranging from 92 to $741 \mu\text{mol} \cdot \text{cm}^{-2} \cdot \text{L}^{-1}$), except for the
364 undoped biochar suggesting from a minimal to a possible total consumption of the reagent (small
365 leaks from the BESs must not be excluded). Also, the consumption of the CO₂ could have occurred
366 due to the precipitation of carbonates (pH > 10), shifting chemical equilibria towards the products of
367 the reaction bicarbonate-carbonate. Likewise, H₂ present in the gasbags is variable according to the
368 case (2 to $31 \mu\text{mol} \cdot \text{cm}^{-2} \cdot \text{L}^{-1}$), except for the CC that shows no H₂. Its absence can be due to the
369 occurrence of parasitic reactions taking place at the electrode interface, leading to the production of
370 C-2 or C-3 compounds [60-63]. As for the CO₂ levels, possible minor leaks in the BESs must be
371 considered

372 Coulombic Efficiency (CE) of methane

373 The production of CH₄ by hydrogenotrophic Archaea in the BESs is connected to the
 374 electrochemically formed H₂. The potential set at -1.2 V vs Ag/AgCl is thermodynamically ideal to
 375 produce H₂ according to many works that use different cathodes that enhance the selectivity towards
 376 the reaction [64-66]. As can be seen from Fig. S6 of Supplementary information, the measured current
 377 densities (mA·cm⁻²) are affected by the nature of the cathode. The 200 h trend (8 days) considers the
 378 average of two replicas and a standard deviation below 5% (error bars not visible in the graph). The
 379 maximum current densities were detected for the composite 20Cu and the undoped biochar (7.8 ± 3.1
 380 mA·cm⁻² and 7.4 ± 0.2 mA·cm⁻², respectively) followed by 10HAP and CC (3.9 ± 0.1 mA·cm⁻² and
 381 2.6 ± 0.1 mA·cm⁻², respectively), and equally by the 5Cu/5HAP and 10Cu/20HAP (1.2 ± 0.1 mA·cm⁻²
 382 ²). With the same applied potential, the presence of HAP increases the resistance of the material,
 383 lowering the current density of a 2 to a 7-fold-factor.

384 From the current densities values, the total number of moles of H₂ that could be electrochemically
 385 produced by the system was calculated following equation 8:

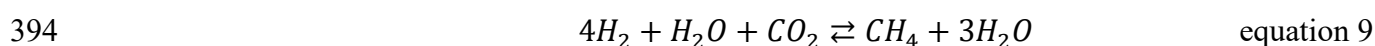
386



388

389 Table 3 summarizes the results obtained in μmoles of H₂ *per* day and cm² of projected surface area,
 390 based on the assumption that the charge supplied was exclusively used for the H₂ evolution reaction.
 391 Assuming that for each mole of CH₄ four moles of H₂ are needed, the electrochemically produced
 392 moles of CH₄ were also calculated (equation 9):

393



395

396 The ideal CH₄ μmoles average from 130 to 850 which is in line with recent literature work on
 397 bioelectrochemical systems [28, 67] using specific materials as cathodes to produce methane. Results
 398 of this experimentation were compared (mmol m² d⁻¹) to the highest CH₄ production available in
 399 literature using CC as a cathode [19] and to the general maximum production of methane in a double
 400 chamber BES [68]. Table 4 displays the average production of CH₄ for each system, the maximum
 401 theoretical CH₄ moles calculated from the electrochemical process, and the Coulombic efficiency
 402 (CE). The CE was calculated according to the following equation:

$$403 \quad CE = \frac{8Fn_{CH_4}}{\int_{t_0}^{t_i} I(t) dt} \quad \text{equation 10}$$

404 where 8 is the number of electrons exchanged in the reaction F is the Faraday constant, n is the number
 405 of moles of CH₄ electrochemically produced and I is the current density circulating for 200h.

406 Most of the BESs show a low methane coulombic efficiency (up to 10%) compared to the moles of
407 CH₄ ideally produced. The average CE varies according to the cathode, showing a minimum value
408 for the CC. Replacing CC with biochar in the cathodic chamber, a two-time increase of the methane
409 bioelectrochemically produced is noticed, suggesting a slightly higher selectivity for the reduction of
410 CO₂ into methane, despite the detection of H₂ in the gasbags. As previously stated, the addition of Cu
411 does not show a significant improvement of methane production which is reflected in a CE
412 comparable to the CC. On the other hand, the presence of HAP enhances the performances of the
413 BESs. Particularly, the composite with 20Cu/10HAP shows production of CH₄ comparable to the one
414 achieved by Gajaraj [19] and Jiang [68]. It is worth mentioning that the production of methane with
415 this new composite is more rapid than the other systems and a value comparable to the maximum
416 methane production available in literature was achieved in less than a quarter of the time (8 days vs
417 30 days or more), in a CO₂ sparging configuration. Also, a good CE (64%) was calculated, suggesting
418 a specific selectivity towards the direct reduction of CO₂ into methane in presence of bacteria [69].

419 Solution analyses

420 Analyses of the concentration of total Volatile Fatty Acids (VFAs) in the solution and pH were carried
421 out before and after each test to verify the occurrence of parasite reaction during the experimentation,
422 made more thermodynamically favoured than the conversion of CO₂ into methane. The microbial
423 transformation of carbon dioxide in organic acids as formates and acetates is one of the possible
424 CO₂RR pathways, specifically when high current densities are supplied [70, 71]. Results for the VFAs
425 concentrations are displayed in Figure 6. Their initial concentration on the pristine inoculum was
426 around 1100 mg L⁻¹, increasing at the end of the test up to more than one order of magnitude. Based
427 on the CE, unwanted or parasite reactions are all taking place in BESs. The CC based system seems
428 the less affected, while biochar cathodes in the BES induce a 10 to 50 folds increase of the VFAs in
429 the solution. As expected, the presence of Cu in the composite (20Cu) catalyses the transformation
430 of CO₂ into C-2 or C-3 hydrocarbons, visible from the high values of VFAs in the solution (50,774
431 mg L⁻¹). Samples with high HAP content (10HAP and 20Cu/10HAP) show comparable values to the
432 pure biochar, indicating that it can positively affect the reaction in terms of selectivity, hindering
433 possible parasitic reactions taking place. However, a low quantity in the mixture (5Cu/5HAP), is not
434 sufficient to contrast those reactions promoted by Cu.

435 The pH in the cathodic chamber was also monitored periodically as displayed in Table 5. Cells with
436 CC, undoped biochar and the 20Cu composite required periodical pH correction due to the H₂
437 produced, therefore pH was lowered with drops of a 0.1 M HCl solution to the initial value. At the
438 end of the test a deposition of white incrustations (not visible), possibly carbonates were visually
439 observed on all cathodes, confirming that the increase of the pH promoted unwanted precipitation on

440 the cathode material of salts from the solution. SEM analyses confirmed the morphology and
441 composition of the precipitation, made primarily of Ca carbonates.

442 Small increases in pH were noted for the systems with HAP, as they remained more stable during the
443 test, thermodynamically favouring methane production [2,72]. Such an optimal control of pH might
444 be ascribed to the peculiar interface behaviour of HAP [47]. Indeed, when in contact with water,
445 hydroxyapatite generates disordered hydrated layers located at the surface and undergoes partial
446 dissolution with the release of its constituting ions (calcium cations, phosphates, and hydroxyl ions).
447 Consequently, the pH at the interface of hydroxyapatite-biochar is buffered by the presence of these
448 ions, in particular various species of phosphates, which impose a pH range between 5.8 and 7.

449 **3.4 Identification of the microorganisms on the biocathodes**

450 To identify the presence of electroactive microorganisms (Archaea and Bacteria) on the cathodes,
451 preliminary SEM observations were carried out on the projected areas exposed to the solution. The
452 micrographs in Fig. 7 show that microorganisms are differently attached on the selected electrodes
453 following the roughness of the surface. Biofilm was observed on all cathodes, more significantly on
454 CC, biochar, 10HAP, and 20Cu (Fig. 7a, b, c, d) while consortia of microorganisms, arranged in
455 concretions were visible on the other composites 5Cu/5HAP and 20Cu/10HAP (Fig. 7e, f).

456 The high porosity of the biochar (macropores) also provides a larger surface for the adhesion of the
457 microorganisms. A preliminary differentiation of microorganisms among the composites can be
458 assessed by the different morphologies observed. The sample 10HAP shows a predominance of
459 filamentous species attached to the surface and close to the HAP aggregates (Fig. 7c). Spherical
460 microorganisms are abundant on the 20Cu biochar substrate, and their attachment follows a first
461 covering of the surface by biofilm (Fig. 7d). A great density of microorganisms was found on the
462 samples 5Cu/5HAP and 20Cu/10HAP, visible as agglomerates (in Fig. 7e, arrows). They bear
463 different morphologies as spherical, rod-shaped, or filamentous (Fig. 7f, at high magnification) and
464 are located predominantly close to and on top of the areas richer in HAP.

465 Fig. 8 and 9 respectively show the graphs of the main genera of Archaea and Bacteria domains from
466 the Next Generation sequencing on V5-V6 16S RNA genes of cathodes samples carried out on the
467 media, before and after the test on all operated cathodes at the end of the test.

468 *Methanobacterium* is the most abundant genus of Archaea for all systems, especially for composite
469 cathodes, enriched with Cu and HAP (more than 90% of relative abundance). It is one of the first
470 known hydrogenotrophic organisms producing methane directly from CO₂. *Methanobrevibacter*,
471 another well-known hydrogenotrophic methanogen, was also found abundantly on carbon cloth
472 (more than 25%) and noticed on the samples 10HAP and 20Cu. *Methanospirillum* was the second

473 abundant hydrogenotrophic methanogen on pure Biochar and was also found on the composites with
474 both Cu and HAP.

475 The graph of bacteria genera in fig. 9 highlights a pronounced difference among the cathodes and
476 from the initial inoculum, enriched with different microorganisms. A multitude of diverse bacteria
477 genera is present in the n the initial anaerobic inoculum picked up from an already enriched pool of
478 hydrogenotropic methanogens.

479 After the experiment, *Thermoanaerobacteraceae* was the most present genus on CC, followed by
480 *Petrobacter*. The first is a large group of common bacteria whose metabolism is greatly variable,
481 ranging from carbohydrate fermentation to chemolithoautotrophy. A decrease of genus variability is
482 noticed for the undoped biochar, the 20Cu and the 10HAP, dominated by *Clostridia* and *Bacilli* (a
483 group of anaerobic fermenters, which can ferment several organic substrates. It is not to exclude that
484 the significant change of pH during the experimentation (from 6.5 to 10 as displayed in Table 5) could
485 have induced more microorganisms' selectivity. In the system 10HAP *Proteiniborus* is also present.
486 Notably, composite cathodes containing both Cu and HAP (5Cu/5HAP and 20Cu/10HAP) are
487 enriched in *Tepidiphilus* phylotypes, which are very active in the transformation and biodegradation
488 of alkanes [73]. On the 20Cu/10HAP sample, the abundance of *Tepidiphilus* was limited by the
489 relevant enrichment of the genus *Proteiniborus*, anaerobic, mesophilic, protein-utilizing bacterial
490 group, which can ferment organics to ethanol, acetic acid, and hydrogen. Comparative phenotypic,
491 chemotaxonomic, and genetic analysis revealed significant similarities among strains of the genus
492 *Tepidiphilus* and *Petrobacter* [74]. It is suggested that the presence of fermentative bacteria
493 contributed to the low quantity of methane detected and that *Tepidiphilus* inhibited the methane
494 production reaction, competing for the transformation of H₂ (system 5Cu/5HAP).

495

496 1. DISCUSSION

497 In bioelectrochemical systems, the pathways of CH₄ formation from CO₂ is still unexplored to a large
498 extent due to the complexity associated to the transfer of 8 e⁻ and the number of microorganisms
499 involved. The metabolic pathways that can lead to the transformation of CO₂ into methane are
500 numerous, often involving a multi-step reaction with different intermediates. The reduction of CO₂
501 into CH₄ by hydrogenotrophic Archaea cannot take place without the presence of sufficient H₂, which
502 theoretically is the rate-limiting step of the overall reaction (4:1 stoichiometric ratio). Opposite to
503 hydrogen, the direct electron uptake from the cathode by these microorganisms requests a high
504 electrochemically active surface as well as controlled local chemical-physical parameters to
505 efficiently produce CH₄. The experimentation of innovative and green cathodes described in this
506 work, based on biochar enriched with Cu and HAP in different quantities, aims to address these

507 requirements: i) selectivity towards the CO₂RR to methane; ii) electrochemically active surface area;
508 iii) control of the pH conditions to an acceptable range for hydrogenotrophic methanogens
509 microorganisms.

510 The support (biochar) was proven to have adequate properties to be used as a biocathode compared
511 to the carbon cloth (CC) in terms of methane productivity: from 3 to an 8-fold increase in presence
512 of 20Cu/10HAP. However, when we look at the coulombic efficiency of the process, only the
513 20Cu/10HAP exhibited a good performance (64% CE). The low production and efficiency of CH₄ at
514 the CC, biochar and 20Cu cathodes, also compared to literature data [19, 68], can be explained by the
515 modification of the pH during the experiment due to the uptake of H⁺ ions from the solution that
516 allowed to produce carbonates, as visually experienced. The equilibrium bicarbonates-carbonates
517 shifts towards the latter when pH increases up to 10, this way inducing the carbonate precipitation on
518 the electrically active sites. This well-known phenomenon leads to the complete deactivation of the
519 cathode, as previously well demonstrated for other types of microbial electrochemical systems [75,
520 76]. The excessive change of the pH led to the proliferation of fermentative microorganisms that: i)
521 promoted alternate metabolic pathways other than the production of methane; ii) transformed the
522 methane produced in organic acids. The competition of different microorganisms on the electrode
523 and the production of different organics by-products could significantly have contributed to the
524 reduction of methane yield compared to other cases.

525 On the other hand, the presence of HAP in the system from a certain amount (10 wt. %) guarantees
526 higher values of methane production, possibly due to: i) its chemical effect on the pH; ii) selectivity
527 towards methane production. It can be supposed that the presence of acidic HAP groups inhibited the
528 increase of the local alkalinity, acting as a buffer [77]. Furthermore, the remarkable adsorption
529 properties of HAP further increase the retention time of the methane production intermediates on the
530 catalyst surface, thus suppressing the generation of CO and HCOO. Wai et al. [78] proved the crucial
531 role of HAP in directing the selectivity, by promoting the formation of hydrogen-carbonate species
532 from CO₂ chemisorption onto O²⁻ ions of the phosphate groups and by stabilizing the bidentate
533 formate species which derive from further hydrogenation of hydrogen-carbonate species. These
534 chemical catalysts mixed in sufficient quantities with graphitic biogenic carbon and deposited on the
535 surface of the biochar cathodes formed a condition that allowed to improve the production of CH₄,
536 being able to preferentially stabilize defined reaction intermediates [47]. The predominance of a
537 different genus here, *Proteiniborus*, whose species generally does not metabolize carbohydrates,
538 alcohols, or fatty acids, but grows in peptone-yeast broth producing ethanol, acetic acid, hydrogen,
539 and carbon dioxide [79] can further indicate the prevalence of different syntrophic metabolisms in this
540 case, which more efficiently led to methane.

541 This is not the case for 5Cu/5HAP, which exhibit the same methane production as CC and the
542 undoped biochar, despite the pH control. This low productivity is of difficult explanation also
543 considering that the presence of basic sites of the HAP on the cathodic sites should exercise the
544 function of reservoirs of adsorbed and pre-activated CO₂, further enhancing the CO₂ conversion to
545 methane. Since the preparation of the composite was not completely successful in the case of
546 5CuNPs/5HAP/C, due to a partial and not total overlapping of the Cu and the HAP, it is possible to
547 assume that the CO₂ produced at the cathode was preferentially catalysed in the areas rich in Cu,
548 where the formation of C-2 and C-3 by-products (e.g. acetates, formates, carboxylates, methanol...) are
549 also enhanced [80, 81]. The relevant presence of these organic compounds was indeed
550 documented in the related electrolytes (Fig. 6). This assumption is also corroborated by the great
551 abundance of methylotroph *Tepidiphilus* phylotypes on these cathodes, well known to degrade
552 alkanes [73]. Hypothesizing the absence of alkanes, it can be assumed that the C-1 C-2 compounds
553 produced on the cathode could have enhanced the bacteria metabolism that competed with the
554 hydrogenotrophic production of methane by Archaea.

555 A final remark concerns the cathodic active area. As indicated by the results, the undoped biochar
556 and the 20Cu produced 3 times higher current density than the CC (7.4 ± 0.2 vs 2.6 ± 0.1 mA·cm⁻²),
557 thus ideally increasing 3 times the H₂ content (and consequently of CH₄) available at the electrode,
558 probably due to a bigger specific projected area (macropores). However, for the composites, the
559 presence of insulating HAP (resistivity of HAP is in the order of 10⁹ Ω·cm vs few Ω·cm of the biochar
560 [32, 82]) increased the electrode resistivity lowering the current density circulating in the cells at 3.9
561 ± 0.1 mA·cm⁻² (10HAP) and 1.2 ± 0.1 mA·cm⁻² (5Cu/5HAP and 20Cu/10HAP) The electrochemical
562 analysis confirms that this outcome is related to both this effect and the actual electrochemical active
563 surface area (ECSA) of the electrode, lowered by a homogeneous dispersion of HAP nanoparticles
564 on the surface of the material. The presence of Cu which should increase this last parameter
565 (particularly for the sample 20Cu/10HAP) has no beneficial effect. This fact could be partially
566 explained by i) the absence of a network of Cu nanoparticles on the surface that could better distribute
567 the charge; ii) the covering of Cu nanoparticles by HAP that are located at the interface with the
568 solution, partially suppressing the charge flow.

569 Although the supplementation of Cu and HAP as a composite material lowers the current density,
570 thus the ECSA, this parameter less affects the production of methane compared to the composition
571 of the electrode. Indeed, both the active phase and the dopant contribute to: i) the selectivity of the
572 reaction; ii) faster kinetics; iii) a more efficient coulombic efficiency. From the perspective of a scale-
573 up of the technology, further research will be dedicated to the production of a more conductive
574 composite electrode enhancing the concentration of Cu and HAP at the interface with the solution,

575 allowing to create a network that could better transfer the charge for the bioelectrochemical
576 production of methane.

577

578 **5. Conclusion**

579 Innovative composite biochar-based cathodes with Cu nanoparticles and Hydroxyapatite
580 (20Cu/10HAP) are successfully tested in this work, for the first time in the literature, to enhance the
581 electromethanogenesis process in double-chamber BES. The significant differences in methane yield
582 and faradic efficiency observed between the different types of biocathodes can be ascribed to the
583 crucial role that Cu nanoparticles and hydroxyapatite dispersed on the biochar surface express in
584 terms of CO₂ reduction reaction catalysis toward C-1 and C-2 compounds and pH stabilization.
585 Proliferation of hydrogenotrophic archaea of *Metanobacterium* genus, in possible syntropy with
586 different genera of fermenting bacteria depends on the cathode type and its functionalization. Porous
587 biochar enriched with 20% Cu and 10% hydroxyapatite showed higher electrochemical performance
588 and biomethane production compared with less enriched biochar, undoped biochar and carbon cloth
589 cathodes. The productivity of methane ($866 \pm 199 \text{ mmol} \cdot \text{m}^{-2} \cdot \text{d}^{-1}$ cathode projected area) was
590 comparable to the maximum obtained in literature in a double chamber BES (1103 and 1159 $\text{mmol} \cdot \text{m}^{-2} \cdot \text{d}^{-1}$
591 cathode projected area respectively with a CC and a carbon felt electrode). Although these
592 experiments had a lower faradaic efficiency (64% vs 90%) these outcomes were achieved in less than
593 a quarter of the time (8 days vs 30 days or more), hypothesizing faster kinetics of production. It is
594 important to underline that the performance of the cathode was determined by the external surface
595 area only, while the internal porous surface of biochar remained almost non-functionalized and was
596 not colonized. Addressing effort in building more uniformly functionalized biochar-based electrode,
597 the methane productivity would be hence further increased.

598

599

600

601 **6. FIGURE CAPTIONS**

602 Figure 1. Schematic of a BES (a), and images of operating BES in the experimented set-up (b and c).

603 Figure 2. Macro and SEM-SE observations of maize stalk sample before and after pyrolysis.

604 Figure 3. SEM-SE micrographs with EDS spectra in point x: a) 5Cu/5HAP (S1 EDS); b)
605 20Cu/10HAP (S2 EDS).

606 Figure 4. SEM elemental mapping of electrodes: a) 5Cu/5HAP; b) 20Cu/10HAP. red=C; orange=P;
607 yellow=Ca; green=Cu.

608 Figure 5. CO₂, H₂ and CH₄ concentration inside the gas bags after 200h (8 days) of test.

609 Figure 6. Total Volatile Fatty Acids measured in the cathodic compartment at the end of the test (200
610 h).

611 Figure 7. SEM micrographs of microorganisms on: a) CC; b) biochar; c) 10HAP; d) 20Cu; e)
612 5Cu/5HAP; f) 20Cu/10HAP.

613 Figure 8 Main genera of Archaea from the NG sequencing of cathodes samples. *Methanobacterium*
614 is the most abundant genus for all cases.

615 Figure 9. Main genera of Bacteria from the NG sequencing of cathodes samples. The most abundant
616 genus for each cathode type is highlighted. Inoculum: Other Genera; CC:
617 Undefined_Thermoanaerobacteraceae; Biochar: *Clostridium XI*; 10HAP: *Bacillus*; 20Cu:
618 *Proteiniborus*; 5Cu/5HAP: *Tepidiphilus*; 20Cu/10HAP: *Proteiniborus*.

619

620 ACKNOWLEDGEMENTS

621 This work was financed by the Research Fund for the Italian Electrical System in compliance with
622 the Decree of March, 19th 2018.

623

624 DATA AVAILABILITY

625 The raw/processed data required to reproduce these findings cannot be shared at this time due to
626 technical or time limitations.

627

628 REFERENCES

629 [1] Geppert F, Liu D, Eerten-Jansen M, Weidner E, Buisman C, Heijne A. Bioelectrochemical Power-
630 to-Gas: State of the Art and Future Perspectives. Trends Biotechnol 2016; 34(11):879-94.

631 [2] Blasco-Gomez R, Batle-Vilanova P, Villano M, Balaguer M, Colprin J, Puig S. On the Edge of
632 Research and Technological Application: A Critical Review of Electromethanogenesis. Int J
633 Mol Sci 2017; 18 (32):874-905.

634 [3] Clauwaert P, Tolêdo R, van der Ha D, Crab R, Verstraete W, Hu H, Udert KM, Rabaey K.
635 Combining biocatalyzed electrolysis with anaerobic digestion. Water Sci Technol
636 2008;57(4):575-579.

637 [4] Clauwaert P, Verstraete W, Methanogenesis in membraneless microbial electrolysis cells. Appl
638 Microbiol Biotechnol 2009;82:829-36.

639 [5] Götz M, Lefebvre J, Mörs F, McDaniel Koch A, Graf F, Bajohr S, Reimert R, Kolb T. Renewable
640 Power-to-Gas: A technological and economic review. Renew En 2016; 85:1371-1390.

- 641 [6] Ning X, Lin R, O'Shea R, Wall D, Deng C, Wu B, Murphy JD. Emerging bioelectrochemical
642 technologies for biogas production and upgrading in cascading circular bioenergy systems.
643 *iScience* 2021; 24(9):102998.
- 644 [7] Aryal N, Kvist T, F. Amman, Pant D, Ottosen LD. An overview of microbial biogas enrichment.
645 *Biores Technol* 2018; 264:359-69.
- 646 [8] Rozzi E, Minuto FD, Lanzini A, Leone P. Green Synthetic Fuels: Renewable Routes for the
647 Conversion of Non-Fossil Feedstocks into Gaseous Fuels and Their End Uses. *Energies* 2020;
648 13 (420) doi:10.3390/en13020420
- 649 [9] Das S, Raj R, Das S, Ghangrekar MM. A Sustainable Approach for the Production of Green
650 Energy With the Holistic Treatment of Wastewater Through Microbial Electrochemical
651 Technologies: A Review. *Front. Sustain.* 2021; doi: 10.3389/frsus.2021.792028
- 652 [10] Benato A, Macor A. Italian Biogas Plants: Trend, Subsidies, Cost, Biogas Composition and
653 Engine Emissions. *Energies* 2019;v12(6):979 doi: 10.3390/en12060979.
- 654 [11] Brémond U, Bertrandias A, Steyer J-P, Bernet N, Carrere H. A vision of European biogas sector
655 development towards 2030: Trends and challenges. *J Cleaner Prod* 2021; 287:125065.
- 656 [12] Beese-Vasbender PF, Grote JP, Garrelfs J, Stratmann M, Mayrhofer KJ. Selective microbial
657 electrosynthesis of methane by a pure culture of a marine lithoautotrophic archaeon.
658 *Bioelectrochem.* 2015; 102:50-5.
- 659 [13] Ferry JG, Fundamentals of methanogenic pathways that are key to the biomethanation of
660 complex biomass. *Curr Opin Biotechnol* 2011;22(3):351-7.
- 661 [14] Thauer RK, Jungermann K, Decker K. Energy conservation in chemotrophic anaerobic bacteria.
662 *Bacteriol Rev* 1977; 41(1):100–80
- 663 [15] Garcia J-L, Patel B, Ollivier B. Taxonomic, phylogenetic and ecological diversity of
664 methanogenic Archaea. *Anaerobe* 2000; 6:205-26.
- 665 [16] Liu Y, Whitman W. Metabolic, phylogenetic, and ecological diversity of the methanogenic
666 Archaea. *Ann N Y Acad Sci* 2008; 1125:171-89.
- 667 [17] Lever M, A New Era of Methanogenesis Research. *Trends Microbiol* 2016; 24(2):84-6.
- 668 [18] Sousa F, Thiergart T, Landan G, Nelson-Sathi S, Pereira I, Allen J, Lane N, Martin W, Early
669 bioenergetic evolution. *Philos Trans R Soc B: Biol Sci* 2013; 368(1622):20130088.
- 670 [19] Gajaraj S, Huang Y, Zheng P, Hu Z. Methane production improvement and associated
671 methanogenic assemblages in bioelectrochemically assisted anaerobic digestion. *Biochem Eng*
672 *J.* 2017; 117:105-12.

- 673 [20] Fu Q, Kuramochi Y, Fukushima N, Maeda H, Sato K, Kobayashi H. Bioelectrochemical
674 Analyses of the Development of a Thermophilic Biocathode Catalyzing
675 Electromethanogenesis. *Environ Sci Technol* 2015; 49(2):1225–32.
- 676 [21] Park DH, Laivenieks M, Guettler MV, Jain MK, Zeikus JG. Microbial utilization of electrically
677 reduced neutral red as the sole electron donor for growth and metabolite production. *Appl
678 Environ Microbiol* 1999; 65(7):2912-7.
- 679 [22] Wang B, Liu W, Zhang Y, Wang A. Natural solar intermittent-powered electromethanogenesis
680 towards green carbon reduction, *Chem Eng J* 2022; 432:134369.
- 681 [23] Gao T, Zhang H, Xu X, Teng J. Mutual effects of CO₂ absorption and H₂-mediated
682 electromethanogenesis triggering efficient biogas upgrading. *Sci Tot Environm* 2022;
683 818:151732.
- 684 [24] Liu D, Zhang L, Chen S, Buisman C, Ter Heijne A. Bioelectrochemical enhancement of methane
685 production in low temperature anaerobic digestion at 10 °C. *Water Res* 2016;99:281-7.
- 686 [25] Guo X, Liu J, Xiao B. Bioelectrochemical enhancement of hydrogen and methane production
687 from the anaerobic digestion of sewage sludge in single-chamber membrane-free microbial
688 electrolysis cells. *Int J Hydr En* 2013; 38(3):1342-1347.
- 689 [26] Dang Y, Holmes DE, Zhao Z, Woodard TL, Zhang Y, Sun D, Wang LY, Nevin KP, Lovley DR,
690 Enhancing anaerobic digestion of complex organic waste with carbon-based conductive
691 materials. *Bioresour Technol* 2016; 220:516–22.
- 692 [27] Molognoni D, Bosch-Jimenez P, Rodríguez-Alegre R, Marí-Espinosa A, Licon E, Gallego J,
693 Lladó S, Borràs E, Della Pirriera M. How Operational Parameters Affect
694 Electromethanogenesis in a Bioelectrochemical Power-to-Gas Prototype. *Front Energy Res*
695 2020; 8:174 doi: 10.3389/fenrg.2020.00174.
- 696 [28] Siegert M, Yates MD, Call DF, Zhu X, Spormann A, Logan BE. Comparison of Nonprecious
697 Metal Cathode Materials for Methane Production by Electromethanogenesis. *ACS Sustainable
698 Chem Eng* 2014; 2:910–7.
- 699 [29] Yuan H-Y, Ding L-J, Fru Zama E, Liu P-P, Hozzein WN, Zhu Y-G. Biochar Modulates
700 Methanogenesis through Electron Syntrophy of Microorganisms with Ethanol as a Substrate.
701 *Environ Sci Technol* 2018; 52 (21):12198–207.
- 702 [30] Viggì CC, Simonetti S, Palma E, Pagliaccia P, Braguglia C, Fazi S, Baronti S, Navarra M, Pettiti
703 I, Koch C, Harnisch F, Aulenta F. Enhancing methane production from food waste fermentate
704 using biochar: the added value of electrochemical testing in pre-selecting the most effective
705 type of biochar. *Biotechnol Biofuels* 2017; 10:303.

- 706 [31] Schievano A, Goglio A, Erckert C, Marzorati S, Rago L, Cristiani P. Organic waste and
707 bioelectrochemical systems: a future interface between electricity and methane distribution
708 grids. *Detritus* 2018; 1:57-63.
- 709 [32] Cristiani P, Goglio A, Marzorati S, Fest-Santini S, Schievano A. Biochar-Terracotta Conductive
710 Composites: New Design for Bioelectrochemical Systems. *Front En Res* 2020; 8
711 doi.org/10.3389/fenrg.2020.581106.
- 712 [33] Jiang Q, Zhang C, Wu P, Ding P, Zhang Y, Cui M-h, Liu H. Algae biochar enhanced
713 methanogenesis by enriching specific methanogens at low inoculation ratio during sludge
714 anaerobic digestion. *BioresTechnol* 2021; 338:12549314.
- 715 [34] Zhang L, Lim EY, Loh K-C, Ok YS, Lee JTE, Shen Y, Wang C-H, Dai Y, Tong YW. Biochar
716 enhanced thermophilic anaerobic digestion of food waste: Focusing on biochar particle size,
717 microbial community analysis and pilot-scale application. *En Convers Management* 2020;
718 209:112654.
- 719 [35] Lu Q, Jiao F. Electrochemical CO₂ reduction: Electrocatalyst, reaction mechanism, and process
720 engineering. *Nano Energy* 2016; 29:439–56.
- 721 [36] Rendón-Calle A, Builes S, Calle-Vallejo F. A brief review of the computational modeling of
722 CO₂ electroreduction on Cu electrodes. *Curr Opin Electrochem* 2018; 9:158-65.
- 723 [37] Hori Y, Murata A, Takahashi R. Formation of hydrocarbons in the electrochemical reduction of
724 carbon dioxide at a copper electrode in aqueous solution. *J Chem Soc Faraday Trans 1 Phys*
725 *Chem Condens Phases* 1989; 85:2309–26.
- 726 [38] Song Y, Peng R, Hensley DK, Bonnesen PV, Liang L, Wu Z, Meyer HM, Chi M, Ma C, Sumpter
727 BG, Rondinone AJ. High-Selectivity Electrochemical Conversion of CO₂ to Ethanol using a
728 Copper Nanoparticle/N-Doped Graphene Electrode. *Chem Select* 2016; 1:6055–61.
- 729 [39] Xie H, Wang T, Liang J, Li Q, Sun S. Cu-based nanocatalysts for electrochemical reduction of
730 CO₂, *Nano Today*. 2018; 21:41–54.
- 731 [40] Baturina OA, Lu Q, Padilla MA, Xin L, Li W, Serov A, Artyushkova K, Atanassov P, Xu F,
732 Epshteyn A, Brintlinger T, Schuette M, Collins GE. CO₂ electroreduction to hydrocarbons on
733 carbon- supported Cu nanoparticles. *ACS Catal* 2014; 4:3682–95.
- 734 [41] Zhao S, Wang DW, Amal R, Dai L. Carbon-Based Metal-Free Catalysts for Key Reactions
735 Involved in Energy Conversion and Storage. *Adv Mater* 2019; 31:1–22.
- 736 [42] Wang X, Feng X, Shang J, Jin Y, Zhang C. Photocatalytic Reduction of CO₂ Using Titanium-
737 Substituted and Fluorine-Doped Titanium-Substituted Hydroxyapatite as Photocatalysts. *Catal*
738 *Letters* 2017; 147:2706–13.

- 739 [43] Kattimani VS, Kondaka S, Lingamaneni KP. Hydroxyapatite—Past, Present, and Future in Bone
740 Regeneration. *Bone Tissue Regen Insights*. 2016;. doi:10.4137/BTRI.S36138.
- 741 [44] Singh G, Singh RP, Jolly SS. Customized hydroxyapatites for bone-tissue engineering and drug
742 delivery applications: a review. *J Sol-Gel Sci Technol* 2020; 94:505-30.
- 743 [45] Souza FS, Matos MJS, Galvão BRL, Arapiraca AFC, Silva SN, Pinheiro IP. Adsorption of CO₂
744 on biphasic and amorphous calcium phosphates: An experimental and theoretical analysis,
745 *Chem Phys Lett* 2019; 714:143–8
- 746 [46] Sans J, Arnau M, Sanz V, Turon P, Alemán C. Hydroxyapatite-based biphasic catalysts with
747 plasticity properties and its potential in carbon dioxide fixation. *Chem Eng J* 2022;
748 433(2):133512.
- 749 [47] Ferri M, Delafontaine L, Guo S, Asset T, Cristiani P, Campisi S, Gervasini A, Atanassov P.
750 Steering Cu-based CO₂RR Electrocatalysts Selectivity: the Effect of Hydroxyapatite
751 Acid/Base Moieties in promoting Formate Production *ACS Energy Letters* 2022; 7: 2304–10.
- 752 [48] Ferri M, Campisi S, Polito L, Shen J, Gervasini A. Tuning the sorption ability of
753 hydroxyapatite/carbon composites for the simultaneous remediation of wastewaters containing
754 organic-inorganic pollutants. *J Hazard Mater* 2021 doi: 10.1016/j.jhazmat.2021.126656.
- 755 [49] Iannucci L, Parvis M, Cristiani P, Ferrero R, Angelini E, Grassini S. A Novel Approach for
756 Microbial Corrosion Assessment, *IEEE Trans. Instrument. Meas.* 2019; 68(5):1424-31, doi:
757 10.1109/TIM.2019.2905734
- 758
- 759 [50] Schindelin J, Arganda-Carreras I, Frise E, Kaynig V, Longair M, Pietzsch T, Preibisch S, Rueden
760 C, Saalfeld S, Schmid B, Tinevez J-Y, White DJ, Hartenstein V, Eliceiri K, Tomancak P,
761 Cardona A. Fiji: an open-source platform for biological-image analysis. *Nat Methods* 2012;
762 9(7):676-82.
- 763 [51] Yaashika PR, Senthil Kumar P, Varjani S, Saravanan A. A critical review on the biochar
764 production techniques, characterization, stability and applications for circular bioeconomy.
765 *Biotechnol Reports* 2020; 28: e00570.
- 766 [52] Koutsoukos PG, Nancollas GH. The morphology of hydroxyapatite crystals grown in aqueous
767 solution at 37°C. *J Cryst Growth* 1981; 55(2):369-75.
- 768 [53] Keiluweit M, Nico PS, Johnson MG, Kleber M. Dynamic molecular structure of plant biomass-
769 derived black carbon (biochar). *Environ. Sci. Technol.* 2010;44:1247–53.
- 770 [54] Trasatti S, Petrii OA. Real surface area measurements in electrochemistry. *Pure Appl. Chem.*
771 1991; 63: 711– 34.

- 772 [55] Cuentas-Gallegos AK, Rayón-López N, Mejía LM, Villafán Vidales H, Miranda-Hernández M,
773 Robles M, Muñiz-Soria J. Porosity and Surface Modifications on Carbon Materials for
774 Capacitance Improvement. *Mesoporous Biomater.* 2016; 3:51–60.
- 775 [56] Baughman RH, Cui C, Zakhidov AA, Iqbal Z, Barisci JN, Spinks GM, Wallace GG, Mazzoldi
776 A, De Rossi D, Rinzler AG, Jaschinski O, Roth S, Kertesz M. Carbon Nanotube Actuators.
777 *Science* 1999; 284:1340–4.
- 778 [57] Barbieri O, Hahn M, Herzog A, Kötz R. Capacitance limits of high surface area activated carbons
779 for double layer capacitors. *Carbon* 2005; 43:1303–10.
- 780 [58] Ding Y, Wang T, Dong D, Zhang Y. Using Biochar and Coal as the Electrode Material for
781 Supercapacitor Applications. *Front Energy Res* 2019; 7:159 doi: 10.3389/fenrg.2019.00159;
- 782 [59] Ji H, Zhao X, Qiao Z, Jung J, Zhu Y, Lu Y, Zhang LL, MacDonald AH, Ruoff RS. Capacitance
783 of carbon-based electrical double-layer capacitors. *Nat Commun* 2014; 5
784 doi:10.1038/ncomms4317.
- 785 [60] Nitopi, S, Bertheussen E, Scott SB, Liu X, Engstfeld AK, Horch S, Seger B, Stephens IEL, Chan
786 K, Hahn C, Nørskov JK, Jaramillo TF, Chorkendorff I. Progress and Perspectives of
787 Electrochemical CO₂ Reduction on Copper in Aqueous Electrolyte. *Chem. Rev.* 2019; 119
788 (12): 7610–72.
- 789 [61] Reske R, Mistry H, Behafarid, F, Roldan Cuenya B, Strasser P. Particle Size Effects in the
790 Catalytic Electroreduction of CO₂ on Cu Nanoparticles. *J. Am. Chem. Soc.* 2014;
791 136(19):6978– 86.
- 792 [62] Baturina OA, Lu Q, Padilla MA, Xin L, Li W, Serov A, Artyushkova K, Atanassov P, Xu F,
793 Epshteyn A, Brintlinger T, Schuette M, Collins GE. CO₂ Electroreduction to Hydrocarbons on
794 Carbon-Supported Cu Nanoparticles. *ACS Catal.* 2014;4(10): 3682–95.
- 795 [63] Loiudice A, Lobaccaro P, Kamali EA, Thao T, Huang BH, Ager JW, Buonsanti R. Tailoring
796 Copper Nanocrystals towards C₂ Products in Electrochemical CO₂ Reduction. *Angew. Chem.,*
797 *Int. Ed.* 2016; 55(19):5789–92.
- 798 [64] Ju HK, Badwal S, Giddey S. A comprehensive review of carbon and hydrocarbon assisted water
799 electrolysis for hydrogen production. *Appl. Energy* 2018; 231: 502-33
- 800 [65] Çelik D, Meltem Y. Investigation of hydrogen production methods in accordance with green
801 chemistry principles. *Int. J. Hydrogen Energy* 2017; 42:23395–401.
- 802 [66] Coughlin RW, Farooque M. Hydrogen production from coal, water and electrons. *Nature*
803 1979;279: 301–3.

- 804 [67] Baek G, Shi L, Rossi R, Logan BE. Using copper-based biocathodes to improve carbon dioxide
805 conversion efficiency into methane in microbial methanogenesis cells. *Chem Eng J* 2022;
806 435:135076.
- 807 [68] Jiang Y, Su M, Zhang Y, Zhan G, Tao Y, Li D. Bioelectrochemical systems for simultaneously
808 production of methane and acetate from carbon dioxide at relatively high rate, *Int. J. Hydrogen*
809 *Energy* 2013; 38:3497-502.
- 810 [69] Pečar D, Goršek A. Kinetics of methane production during anaerobic digestion of chicken
811 manure with sawdust and miscanthus, *Biomass Bioen.* 2020; 143:105820.
- 812 [70] May HD, Evans PJ, LaBelle EV. The bioelectrosynthesis of acetate, *Curr. Op. Biotechnol.*2016;
813 42:225-33.
- 814 [71] Tian Y, Li D, Liu G, Li C, Liu J, Wu J, Liu J, Feng Y. Formate production from CO₂
815 electroreduction in a salinity-gradient energy intensified microbial electrochemical system,
816 *Biores. Technol.* 2021; 320A:124292.
- 817 [72] Pawar AA, Karthic A, Lee S, Pandit S, Jung SP. Microbial electrolysis cells for
818 electromethanogenesis: Materials, configurations and operations. *Environ Eng Res* 2022;
819 27(1):200484
- 820 [73] Liu Y-F, Chen J, Liu Z-L, Hou Z-W, Liang B, Wang L-Y, Zhou L, Shou L-B, Lin D-D, Yang
821 S-Z, Liu J-F, Wu X-L, Gu J-D, Mu B-Z. Long-term cultivation and meta-omics reveal
822 methylotrophic methanogenesis in hydrocarbon-impacted habitats. *Engineering* 2022; doi:
823 10.1016/j.eng.2021.08.027
- 824 [74] Poddar A, Lepcha RT, Das SK. Taxonomic study of the genus *Tepidiphilus*: transfer of
825 *Petrobacter succinatimandens* to the genus *Tepidiphilus* as *Tepidiphilus succinatimandens*
826 *comb. nov.*, emended description of the genus *Tepidiphilus* and description of *Tepidiphilus*
827 *thermophilus* sp. nov., isolated from a terrestrial hot spring”, *Int J Syst Evolution Microbiol*
828 2014; 64:228–35.
- 829 [75] Santini M, Marzorati S, Fest-Santini S, Trasatti SP, Cristiani P. Carbonate scale deactivating the
830 biocathode in a microbial fuel cell. *J Power Sources*; 2017; 356:400-407.
- 831 [76] Santini M, Guilizzoni M, Lorenzi M, Atanassov P, Marsili E, Fest-Santini S, Cristiani P, Santoro
832 C. Three-Dimensional X-ray Micro Computed Tomography Of Carbonates And Biofilm On
833 Operated Cathode In Single Chamber Microbial Fuel Cell. *Biointerphases* 2015; 10(3):031009.
- 834 [77] Dileep Kumar VG, Sridhar MS, Aramwit P, Krut'ko VK, Musskaya ON, Glazov IE, Reddy N.
835 A review on the synthesis and properties of hydroxyapatite for biomedical applications. *J*
836 *Biomater Sci Polym Ed.* 2022; 33(2):229-61. doi: 10.1080/09205063.2021.1980985.

- 837 [78] Wai MH, Ashok J, Dewangan N, Das S, Xi S, Borgna A, Kawi S. Influence of Surface Formate
838 Species on Methane Selectivity for Carbon Dioxide Methanation over Nickel Hydroxyapatite
839 Catalyst, *Chem. Cat. Chem.* 2020; 12: 6410–19, doi.org/10.1002/cctc.202001300
- 840 [79] Niu L, Song L, Dong X. *Proteiniborus ethanoligenes* gen. nov., sp. nov., an anaerobic protein-
841 utilizing bacterium. *Int J Syst Evol Microbiol* 2008;58(Pt 1):12-6.
- 842 [80] Schouten KJP, Kwon Y, Van Der Ham CJM, Qin Z, Koper MTM. A new mechanism for the
843 selectivity to C1 and C2 species in the electrochemical reduction of carbon dioxide on copper
844 electrodes. *Chem Sci* 2011; 2:1902–9.
- 845 [81] Nie X, Esopi MR, Janik MJ, Asthagiri A. Selectivity of CO₂ reduction on copper electrodes:
846 The role of the kinetics of elementary steps. *Angew Chemie - Int Ed* 2013; 52:2459–62.
- 847 [82] Ben Osman M, Krafft JM, Millot Y, Averseng F, Yoshioka T, Kubo J, Costentin G. Molecular
848 Understanding of the Bulk Composition of Crystalline Nonstoichiometric Hydroxyapatites:
849 Application to the Rationalization of Structure–Reactivity Relationships. *European J In Chem*
850 2026; 17: 2709-20.
- 851
852
853